Supporting Information

Hare et al. 10.1073/pnas.1010246107

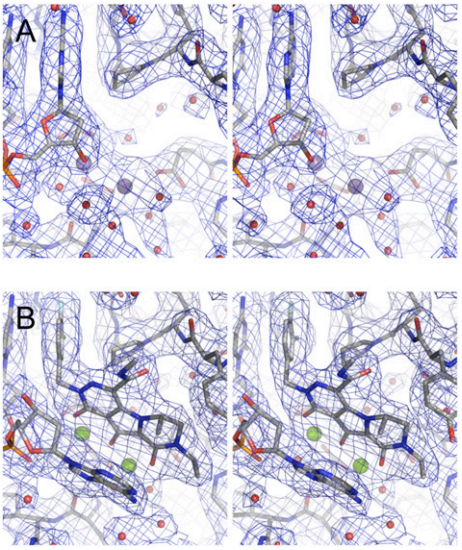

Fig. S1. Wall-eye stereo views of the active site of the PFV intasome bound to Mn^{2+} (*A*) or Mg^{2+}/MK2048 (*B*). Standard atom coloring is used throughout with carbon atoms colored gray. Protein and DNA are shown as stick representation, with Mn (purple) and Mg (light green) atoms shown as large spheres and water molecules as small spheres. The *2Fo-Fc* weighted map contoured at 1σ is shown as a blue mesh.

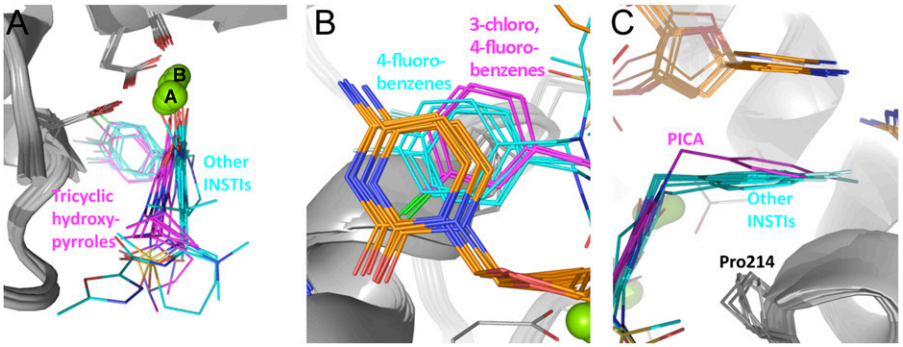

Fig. S2. Comparisons of different INSTIs binding to the PFV intasome. (*A*) INSTI-bound active sites of PFV intasomes viewed along the metal A–metal B axis (a 90° rotation about the vertical axis compared with Fig. 1*C*). The metals are shown as green spheres and the catalytic side chains and INSTIs are shown as sticks. The carbon atoms of tricyclic hydroxypyrroles are colored magenta and those of the other INSTIs are cyan, showing the tilt in the core INSTI ring system. (*B*) Comparison of the interactions between 4-fluoro- (cyan) and 3-chloro,4-fluoro (magenta)-benzene groups of the INSTIs, as viewed from above the penultimate cytosine base of the transferred strand of viral DNA. (*C*) A side view of the π-stacking interaction between INSTI halobenzene groups and the cytosine base. The halobenzene of PICA (magenta) binds at a different angle to the other INSTIs due to an increased distance between it and the metal chelating pharmacophore.

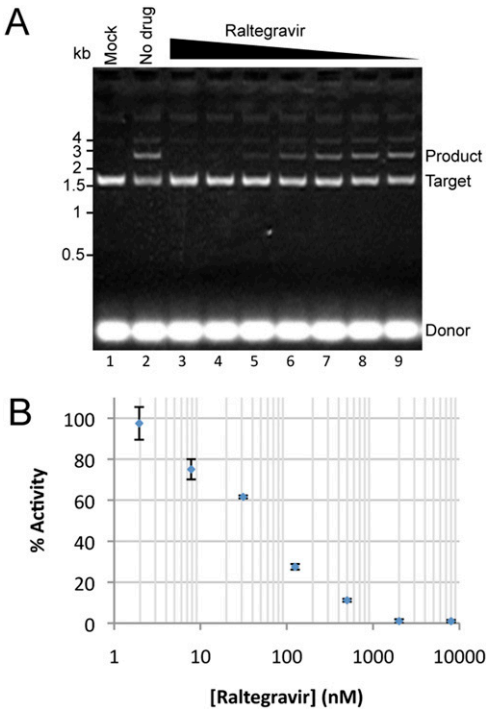

Fig. S3. An example of PFV IN strand transfer assay at a range of raltegravir concentrations. (*A*) Reaction products separated on a 1.5% agarose gel. Migration positions of bands corresponding to donor DNA (a 38-bp mimic of the preprocessed U5 end of PFV DNA), target DNA (supercoiled plasmid), and product (linearized plasmid following concerted integration of two donors) are indicated to the right of the gel image, and the migration position of size standards is indicated to the left. Lane 1 contains the product of a mock reaction with no PFV IN added, and lane 2 shows activity of 0.75 μM PFV IN in the absence of the INSTI. Lanes 3–9 also contain 0.75 μM PFV IN with a titration of raltegravir from 8 μM to 2 nM in a fourfold serial dilution. (*B*) Scatter graph of relative strand transfer activities against raltegravir concentration; activity in the absence of drug was set to 100%. Integration assay products were analyzed by quantitative real-time PCR in triplicate; mean values are shown with error bars indicating SDs.

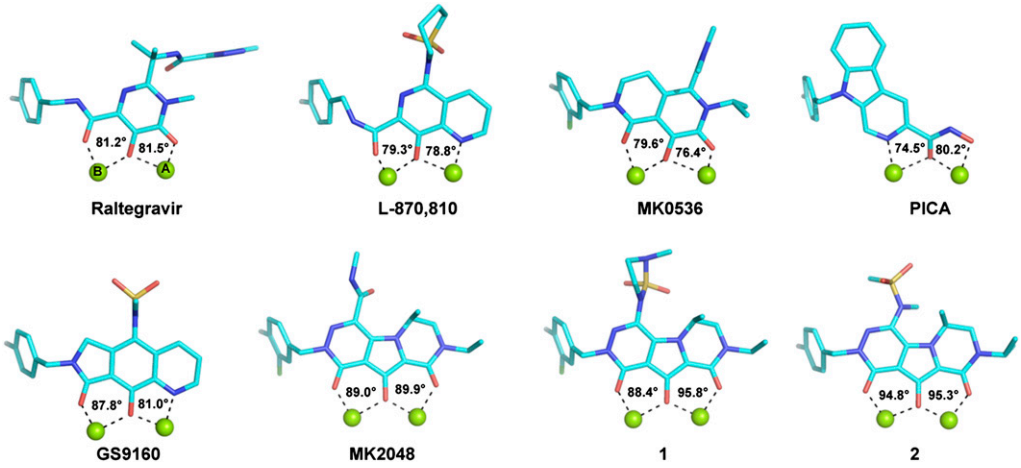

Fig. S4. Coordination of the active site magnesium ions by the INSTIs. For each WT:INSTI complex structure drug molecules are shown as sticks and magnesium ions as green spheres, with drug–metal–drug angles shown.

Table S1. Crystallography data collection and refinement statistics

	WT:Mn	WT:raltegravir	WT:L870,810	WT:MK0536	WT:PICA	WT:GS9160	WT:MK2048	WT:compound1
Data collection*								
Beamline	Diamond I02	Soleil Proximal	Soleil Proximal	Soleil Proximal	SLS X06DA	Soleil Proximal	Soleil Proximal	Soleil Proximal
Space group	$P4_12_12$	$P4_12_12$	$P4_12_12$	$P4_12_12$	P41212	$P4_12_12$	$P4_12_12$	$P4_12_12$
Cell dimensions *a*, *b*, *c*, Å	160.1,160.1,123.9	159.8,159.8,124.1	159.3,159.3,123.3	159.0,159.0,123.7	160.0,160.0,123.8	159.5,159.5,123.6	159.9,159.9,123.3	160.1,160.1,123.5
Resolution range, Å	40–2.55 (2.69–2.55)	40–2.65 (2.79–2.65)	40–2.51 (2.65–2.51)	40–2.74 (2.89–2.74)	40–2.66 (2.80–2.66)	40–2.54 (2.68–2.54)	40–2.54 (2.68–2.54)	40–2.56 (2.70–2.56)
R_{merge}	0.084 (0.931)	0.097 (0.856)	0.100 (0.869)	0.095 (0.880)	0.077 (0.613)	0.108 (1.008)	0.104 (1.044)	0.089 (0.696)
$I/\sigma(I)$	14.1 (2.0)	8.1 (1.6)	10.3 (1.6)	9.8 (1.6)	10.4 (2.0)	8.5 (1.6)	11.6 (1.6)	9.7 (1.6)
Completeness, %	98.9 (99.9)	99.3 (99.2)	96.1 (92.8)	97.8 (99.2)	99.6 (100)	99.8 (99.9)	99.5 (99.6)	97.0 (92.6)
Redundancy	5.5 (5.4)	3.7 (3.6)	5.2 (4.9)	4.7 (4.8)	3.7 (3.7)	5.5 (5.5)	5.4 (5.4)	3.9 (3.6)
Refinement								
Resolution	39.21–2.55	38.02–2.65	38.65–2.51	39.92–2.74	38.8–2.66	39.88–2.54	39.1–2.54	39.15–2.56
Reflections, total/free	49,435/2,627	44,443/2,359	49,439/2,656	39,638/2,098	43,835/2,333	50,084/2,669	50,011/2,668	47,710/2,528
R_{work}/R_{free}	0.197/0.222	0.205/0.228	0.204/0.232	0.203/0.236	0.202/0.226	0.207/0.234	0.204/0.224	0.205/0.227
No. atoms								
Protein	4,339	4,362	4,356	4,343	4,367	4,392	4,343	4,352
Ligand/ion	771	803	801	801	795	800	803	828
Water	274	234	272	162	245	236	252	240
Average B-factors, Å^2								
Protein	58.9	56.4	52.9	69.6	57.3	62.7	54.3	57.1
Ligand/ion	56.3	53.9	50.4	66.8	53.9	59.5	51.1	53.5
Water	54.8	49.7	47.8	59.3	50.1	56.6	48.5	50.0
R.M.S. deviations								
Bond lengths, Å	0.011	0.012	0.011	0.013	0.011	0.012	0.011	0.011
Bond angles, °	1.50	1.56	1.52	1.58	1.48	1.60	1.51	1.49
Ramachandran, %								
Favored	96.5	96.9	96.7	95.6	96.9	96.9	97.1	97.3
Outliers	0	0	0	0	0	0.2	0.2	0
PDB ID	3OY9	3OYA	3OYF	3OYH	3OYC	3OYD	3OYB	3OYG

Table S1. Cont.

	WT:Compound2	S217Q:Mn	S217H:Mn	N224H:Mn	S217Q:MK2048	S217H:MK2048	N224H:MK2048
Data collection*							
Beamline	Soleil Proximal	Diamond I04	Soleil Proximal	Diamond I04	Diamond I04	Soleil Proximal	Diamond I04
Space group	$P4_12_12$	$P4_12_12$	$P4_12_12$	$P4_12_12$	$P4_12_12$	$P4_12_12$	$P4_12_12$
Cell dimensions *a*, *b*, *c*, Å	159.5,159.5,123.1	160.6,160.6,123.5	159.8,159.8,123.9	158.1,158.1,122.2	160.2,160.2,123.7	159.7,159.7,123.5	160.7,160.7,123.1
Resolution range, Å	40–2.74 (2.89–2.74)	40–2.72 (2.87–2.72)	40–2.72 (2.87–2.72)	40–2.02 (2.13–2.02)	40–2.68 (2.82–2.68)	40–2.54 (2.68–2.54)	40–2.68 (2.82–2.68)
R_{merge}	0.154 (0.862)	0.146 (0.864)	0.119 (1.115)	0.106 (0.761)	0.101 (0.894)	0.093 (0.983)	0.096 (1.025)
$I/\sigma(I)$	6.1 (1.6)	6.4 (1.6)	8.4 (1.6)	8.7 (1.6)	11.2 (1.6)	11.7 (1.7)	10.2 (1.6)
Completeness, %	99.6 (99.9)	99.6 (99.9)	98.8 (99.6)	98.9 (98.8)	98.9 (98.9)	99.7 (100)	98.1 (99.0)
Redundancy	4.7 (4.7)	4.6 (4.6)	4.6 (4.7)	4.8 (4.9)	5.5 (5.5)	5.3 (5.4)	5.1 (5.2)
Refinement							
Resolution	39.01–2.74	38.95–2.72	39.15–2.72	39.89–2.02	38.85–2.68	39.09–2.54	38.97–2.68
Reflections, total/free	39,552/2,091	41,260/2,185	40,677/2,151	94,720/5,025	42,639/2,260	50,142/2,676	42,179/2,249
R_{work}/R_{free}	0.204/0.234	0.211/0.243	0.202/0.233	0.198/0.227	0.206/0.241	0.205/0.227	0.208/0.231
No. atoms							
Protein	4,370	4,332	4,319	4,388	4,345	4,346	4,372
Ligand/ion	805	770	770	790	803	803	807
Water	217	205	238	598	198	229	189
Average B-factors, Å^2							
Protein	58.3	63.4	61.0	36.7	63.0	60.2	66.8
Ligand/ion	54.5	57.0	58.2	37.2	60.1	56.9	62.4
Water	49.7	54.6	53.3	46.4	53.0	53.1	57.0
R.M.S. deviations							
Bond lengths, Å	0.012	0.012	0.012	0.010	0.012	0.010	0.011
Bond angles, °	1.56	1.63	1.53	1.35	1.58	1.42	1.49
Ramachandran, %							
Favored	96.9	96.5	95.8	98.7	97.2	97.2	97.6
Outliers	0	0.2	0	0	0.2	0	0.2
PDB ID	3OYE	3OYI	3OYK	3OYM	3OYJ	3OYH	3OYN

*Values in parentheses indicate the highest-resolution shell.

Table S2. Electronic properties of INSTIs

	q_1	q_2	q_3	f_{NN} HOMO	α
Raltegravir	−0.5	−0.62	−0.64	0.357	340.12
L-870,810	−0.58	−0.52	−0.82	0.6774	324.75
MK0536	−0.49	−0.63	−0.62	0.2927	317.05
PICA	−0.73	−0.62	−0.63	0.5746	340.99
GS9160	−0.58	−0.61	−0.71	0.3958	308.96
MK2048	−0.56	−0.68	−0.56	0.4266	358.11
Compound **1**	−0.56	−0.68	−0.58	0.4442	390.46
Compound **2**	−0.58	−0.69	−0.56	0.4003	375.08

Calculated electrostatic potential charges for the three atoms that interact with Mg^{2+} (q_1, q_2, and q_3) are shown. q_1 is the charge on the atom that is closest to the halo-benzyl group, and q_3 is the charge on the atom that is most distant from the halo-benzyl group. f_{NN} HOMO, the atomic Fukui index of the negatively charged oxygen atom that is interacting with Mg^{2+}; α, polarizability. All properties are in atomic units.

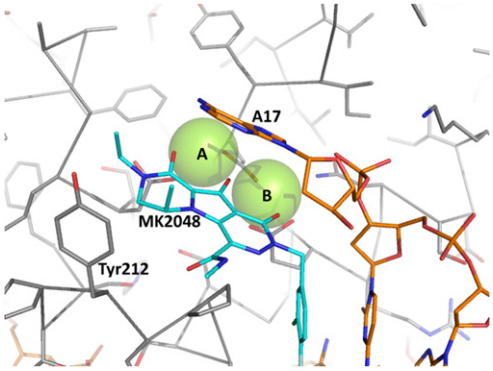

Movie S1. Simulation of MK2048 binding at the active site of WT PFV intasome. The protein chain is shown as a Cα trace. Selected IN residues MK2048 and viral DNA are shown as sticks and indicated; for clarity, 3′ adenosine is only shown in the last frame of the animation.

Movie S1

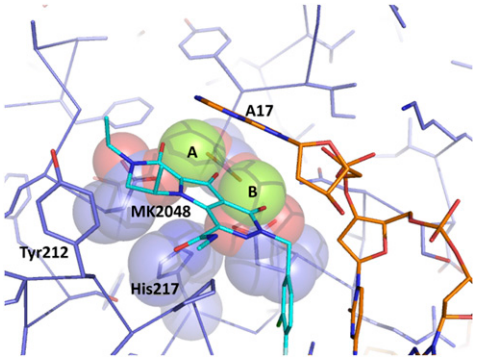

Movie S2. Simulation of MK2048 binding at the active site of S217H PFV intasome. To emphasize the steric interactions necessitating displacement of the mutant His residue in the active site, side chains of selected residues are shown as Van der Waals spheres.

Movie S2

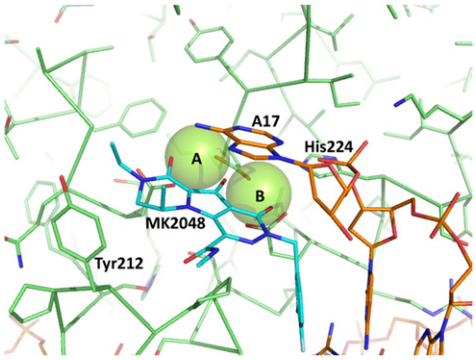

Movie S3. Simulation of MK2048 binding at the active site of N224H PFV intasome. The interaction between mutant His224 and the phosphate group of viral DNA is shown as dashes.

Movie S3